Surface acoustic waves in strain-engineered $K_{0.7}Na_{0.3}NbO_3$ thin films

Sijia Liang, Yang Dai, L. von Helden, J. Schwarzkopf, and R. Wördenweber

Surface acoustic waves in strain-engineered $K_{0.7}Na_{0.3}NbO_3$ thin films

Sijia Liang,[1,a] Yang Dai,[1] L. von Helden,[2] J. Schwarzkopf,[2] and R. Wördenweber[1]

[1]*Institute of Complex System–Bioelectronics (ICS-8), Forschungszentrum Jülich, Jülich 52425, Germany*
[2]*Leibniz Institute for Crystal Growth (IKZ), 12489 Berlin, Germany*

Epitaxial $K_{0.7}Na_{0.3}NbO_3$ thin films are grown via metal-organic chemical vapor deposition on (110)-oriented $TbScO_3$. The films are strained due to the substrate–film lattice mismatch and therefore exhibit a strong and anisotropic modification of all its ferroelectric properties. The compressive in-plane strain leads to a reduction of the ferroelectric transition temperature from approximately 700 K for unstrained $K_{0.7}Na_{0.3}NbO_3$ to 324 K and 330 K with maximum permittivities of 10 270 and 13 695 for the main crystallographic directions $[001]_{TSO}$ and $[1\bar{1}0]_{TSO}$, respectively. Moreover, the quite thin films (approx. 30 nm thick) exhibit very large piezoelectric properties. For instance, surface acoustic waves with intensities of up to 4.7 dB are recorded for wave propagation along the $[1\bar{1}0]_{TSO}$ direction. The signal is smaller (up to 1.3 dB) along $[001]_{TSO}$, whilst for the intermediate direction $[1\bar{1}2]_{TSO}$, the signal seems to vanish (<0.1 dB). The results indicate that the choice of material, $(K,Na)NbO_3$, in combination with strain-engineering via epitaxial growth onto lattice-mismatched substrates represents a promising way to optimize ferroelectric materials for piezoelectric thin-film applications. *Published by AIP Publishing.*
https://doi.org/10.1063/1.5035464

Surface acoustic wave (SAW) devices are widely used today in communications and signal processing, transducers, actuators, and sensors. Recently, novel concepts for bioapplications ranging from highly sensitive and selective QCMs or biosensors, microfluidics, and microactuation to complex lab-on-a-chip devices are increasingly becoming the focus of research on piezoelectric materials and SAW devices.[1–6] One of the main aims of these research activities is to find and optimize systems for various applications. This involves the demand of integrating piezoelectric or SAW components into complex devices. The obvious solution here would be to develop thin-film piezoelectric components that are compatible with other electronics. Obviously, toxic materials should be avoided. $PbZr_{1-x}Ti_xO_3$-based ceramics are widely used in modern electronic devices due to their excellent piezoelectric properties.[7] However, the use of lead has been restricted by the EU, for instance, due to its toxic effects on human health and the environment.[8] Other materials with suitable piezoelectric properties must therefore be found. Finally, these materials have to be fabricated, characterized, and optimized for the given application. This ultimately requires the development and optimization of suitable ferroelectric materials in the form of thin films.

In this study, we demonstrate that extremely thin films of epitaxially grown $(K,Na)NbO_3$ might be suitable for SAW applications. We chose $(K,Na)NbO_3$, a lead-free piezoelectric ceramic with a high piezoelectric performance.[9–13] Values for the piezoelectric constant of $d_{33} \approx 416 pCN^{-1}$ have been reported for Li, Ta, and Sb-modified $(K,Na)NbO_3$ ceramics.[14] Thin epitaxial films of this material are deposited on single crystalline substrates. By choosing a stoichiometry of $K_{0.7}Na_{0.3}NbO_3$, we ensure a large piezoelectric effect, and

the application of metal-organic chemical vapor deposition provides well-ordered epitaxial film growth.[15] Furthermore, by using adequate substrates, in this case (110)-oriented $TbScO_3$, we can induce the adequate strain in the film to adjust the transition temperature from ~700 K (Refs. 10, 16, 17) for the unstrained material to 324–330 K depending on the direction of the electric field.[18,19] This leads to an optimized performance of the thin films around room temperature. Finally, the small anisotropy in the strain leads to a large anisotropy in the propagation of SAWs, which might also be significant for a number of applications.

$K_{0.7}Na_{0.3}NbO_3$ films with a thickness of 25–35 nm are deposited via liquid-delivery spin metal-organic chemical vapor deposition at a temperature of 700 °C onto (110)-oriented single crystalline $TbScO_3$ substrates following the process described in Ref. 15. The structural and stoichiometric properties of the films are analyzed by means of high-resolution X-ray diffraction experiments and time-of-flight secondary ion mass spectrometry (TOF-SIMS), respectively. The structural and compositional analysis reveals that the $K_{0.7}Na_{0.3}NbO_3$ films grow epitaxially in a perfect manner on $TbScO_3$ with the intended stoichiometric composition.[20]

The surface of (110)-oriented $TbScO_3$ is defined by the lattice parameters 2×3.960 Å and 2×3.959 Å along the two in-plane orientations, $[1\bar{1}0]_{TSO}$ and $[001]_{TSO}$,[21] whereas the pseudocubic lattice parameters of bulk $K_{0.7}Na_{0.3}NbO_3$ using Vegard's law are $a_{pc} = 3.954$ Å and $b_{pc} = c_{pc} = 4.014$ Å with a monoclinic distortion angle $\alpha = 89.7°$ between the b_{pc} and c_{pc} axes.[22–24] As a consequence of the epitaxy, the $K_{0.7}Na_{0.3}NbO_3$ film grows c_{pc}-axis-oriented with a strongly compressed b_{pc} axis and a slightly enlarged a_{pc} axis. Moreover, due to the highly regular formation of "superdomains" in the $K_{0.7}Na_{0.3}NbO_3$ film,[20] the orientation of the b_{pc} and a_{pc} axes of the film regularly changes from $[1\bar{1}0]_{TSO}$ to $[001]_{TSO}$. As a consequence of the elastic lattice

a)Author to whom correspondence should be addressed: si.liang@fz-juelich.de

relaxation, the resulting effective in-plain strain in the $K_{0.7}Na_{0.3}NbO_3$ film is compressive and differs slightly (0.025%) for the $[1\bar{1}0]_{TSO}$ and $[001]_{TSO}$ orientations. The observed domain structure and film symmetry are investigated in detail in Ref. 20.

For the electronic characterization (SAW and permittivity) of the films, interdigitated electrodes are fabricated by means of a lift-off technique using electron-beam lithography and metallization consisting of the 5 nm-thick adhesion layer of Ti and a 50 nm-thick layer of Pt.

The layout and orientation of the interdigital transducers (IDT) for the surface acoustic wave experiments are shown in Fig. 1(a). The complete device consists of a generator IDT (input) and a analyzer IDT (output) with identical structures, i.e., 4 finger pairs with 3 μm width and gap size [as shown in Fig. 1(b)], yielding a SAW wavelength of $\lambda = 12\,\mu$m, an effective (free) finger length of 500 μm, and a propagation distance for the SAWs (center-to-center distance between the generator and the analyzer) of $L = 500\,\mu$m [see Fig. 1(a), the arrows indicate the propagation direction of SAW]. The input IDT is driven by an rf signal generator (HP E4422B or Keithley 2920A) in a frequency range from 50 MHz to 3 GHz whilst an input power of typically 0 dBm, and a spectrum analyzer (Anritsu MS2661C or Keithley 2820A) is used to measure the SAW frequency response.

For the investigation of the in-plane dielectric properties, larger interdigitated electrodes (IDE) are added. These IDEs have 32 finger pairs with a width of 10 μm, an effective length of 700 μm, and a gap size of 5 μm.[25] Permittivity is derived from the capacitive signal of the planar IDE capacitor using the partial capacitance model.[26]

All electronic characterizations are performed in a cryostat operating in a temperature range of 5 K to 500 K.

Figure 2 summarizes the SAW data obtained at room temperature for a 27 nm-thick $K_{0.7}Na_{0.3}NbO_3$ film on TbScO$_3$. A complete frequency scan of the response of the interdigital transducers oriented along the $[1\bar{1}0]_{TSO}$ direction is shown in the main plot; the details of the 3rd harmonic, the largest SAW signal, are given in the inset. The figure reveals a number of interesting aspects.

First, only the fundamental and odd harmonic excitations are visible—not the even harmonics. The fundamental SAW signals at the first center frequency $f_1 \approx 275$ MHz are

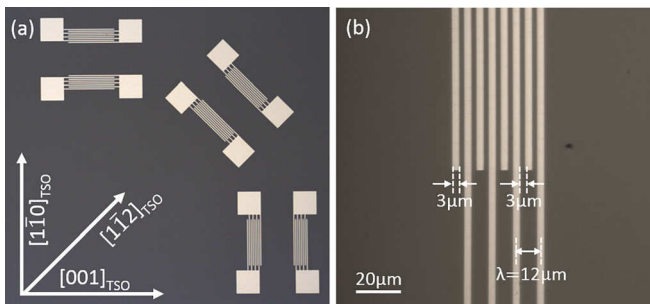FIG. 2. Frequency dependence of the transmission signal of a SAW structure, where $\lambda = 12\,\mu$m and $L = 500\,\mu$m (see Fig. 1), on a 27 nm-thick $K_{0.7}Na_{0.3}NbO_3$ film on (110) TbScO$_3$ measured at room temperature, which exhibits SAW signals for the odd harmonics marked 1st to 9th for the small-strain direction $[1\bar{1}0]_{TSO}$. The inset shows a detailed plot of the signal at the 3rd harmonic (center frequency f_3 indicated by arrows) for the $[1\bar{1}0]_{TSO}$, $[001]_{TSO}$, and $[1\bar{1}2]_{TSO}$ directions of the SAW propagation with respect to the crystalline orientation of the (110) TbScO$_3$ substrate. For better visibility, the signals are shifted by 2 dB for the different directions in (b).

followed by further SAW signals at the odd harmonics 3 to 9 (marked 3rd, 5th, 7th, and 9th in Fig. 2) at center frequencies of about 824 MHz, 1.37 GHz, 1.86 GHz, and 2.34 GHz, respectively. This agrees with the expectation for strong-coupling material and "conventional" IDTs, i.e., IDTs with an identical finger width and finger spacing.[27,28] The electromechanical coupling coefficient K^2 can be obtained from the radiation resistance G_a and susceptance B via the crossed-field model according to $K^2 = \left(\frac{\pi}{4N}\frac{G_a}{B}\right)_{f=f_i}$, with N representing the number of IDT finger pairs.[29] The resulting K^2 values for our film are $(1.4 \pm 0.2)\%$ and $(0.6 \pm 0.1)\%$ for the directions $[1\bar{1}0]_{TSO}$ and $[001]_{TSO}$, respectively. Considering (i) the thinness of our piezoelectric layer (30 nm) and (ii) that the K^2 value strongly decreases with the ratio h/λ (h: thickness of the layer represents an excellent value. The comparison of 800 nm thick LiNbO$_3$ films and 500 nm thick ZnO films showed K^2 factors of 0.52% and $<1\%$, respectively.[30,31] We can therefore conclude that the $K_{0.7}Na_{0.3}NbO_3$ film is a material with a strong piezoelectric coupling expressed by a large coupling coefficient.

Second, the largest signal is observed for the 3rd harmonic. This is rather unusual at first glance. The SAW signal at the different harmonics generally depends on the ratio between the width w and spacing s of the electrode's fingers. For $w/s = 1$, which agrees with our design, the fundamental excitation should generate the largest SAW signal and the intensity should decrease with the order of the higher harmonic.[27] Moreover, in thin-film SAWs, high-order harmonics are usually quite weak.[6] One explanation for this would be the existence of high-order Sezawa-mode waves, which are observed in layered structures in which the substrate has a higher acoustic velocity than the overlaying film.[32,33] The appearance of this type of wave is determined by the ratio of

FIG. 1. (a) Layout and (b) partial image of the interdigital transducers (IDTs) on the $K_{0.7}Na_{0.3}NbO_3$ for the SAW experiments including the crystalline orientation of the different IDTs with respect to the (110)-oriented TbScO$_3$ substrate and the important design parameters. Similar but more extended interdigitated structures and geometric arrangements are used for the measurement of permittivity.[25]
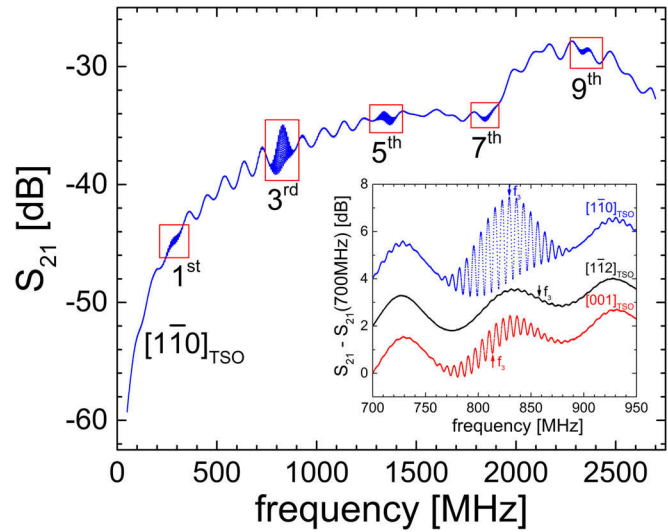
the piezoelectric film thickness h and the SAW wavelength λ. Sezawa waves are usually observed when $h/\lambda > 0.15$.[34,35] However, in our case, $h/\lambda = 0.0025$ is extremely small, and thus, higher-order Sezawa waves are very unlikely to occur.

Another explanation might be the extreme thinness of the piezoelectric layer compared to that of typical thin film SAW devices. At the fundamental frequency, the wavelength (12 μm) is much larger than the film thickness (27 nm). Since the SAW typically penetrates about one wavelength into the free surface, only a small fraction of the mechanical energy can be stored in our very thin $K_{0.7}Na_{0.3}NbO_3$ film, whilst a large fraction is damped in the non-piezoelectric $TbScO_3$ substrate. This situation changes with the higher harmonics. At the 3rd harmonic, the wavelength is already 3 times smaller and the energy is generally more concentrated at the surface, meaning that a larger amount of the SAW energy is concentrated in the film. As a result, the percentage of SAW energy stored in the thin film increases with the order of harmonics, whilst the general signal height decreases with increasing order. This leads to a maximum of the SAW signal for the 3rd harmonic.

Third, the SAW signal is strongly anisotropic. The inset of Fig. 2 provides detailed plots of the device signal at the 3rd harmonic for SAWs propagating along different orientations of the device. For better visibility, S_{21} is normalized and vertically shifted for the different measurements. The black arrows denote the respective center frequencies f_3 for the different directions. The velocity v of the SAW is obtained from the center frequency and the wavelength λ according to $v = (f_n \cdot \lambda)/n$ with n representing the order of harmonics. According to this equation, we obtain slightly different SAW velocities for the different directions: 3277 m/s, 3296 m/s, and 3419 m/s for $[001]_{TSO}$, $[1\bar{1}0]_{TSO}$, and $[1\bar{1}2]_{TSO}$, respectively. Furthermore, the velocity slightly decreases with the harmonic order (see details in the supplementary material). These values are comparable to the velocities measured for classical SAW materials such as $LiNbO_3$, $LiTaO_3$, and quartz.

The SAW spectrum around the center frequency shows the typical interference pattern with a periodicity of about 6.7 MHz. This can be attributed to the interference of acoustic and electromagnetic waves. The signal at the output IDT consists of two components: the directly coupled electromagnetic signal from the input IDT and the electric signal converted from the acoustic wave. The difference in velocity between acoustic and electromagnetic waves leads to a phase difference between the two components and therefore to the observed interference pattern with a periodicity of $\Delta f = v/L$, where L represents the distance between input IDT and output IDT. Inserting the SAW velocity yields an expected periodicity of (6.68 ± 0.15) MHz, which agrees perfectly with the experimental observation.

In order to analyze the SAW signal and its anisotropy further, we plotted the amplitude of the SAW interference pattern around the 3rd harmonic (Fig. 3). The amplitude ΔS_{21} is defined by the peak-to-valley value within the interference pattern (see inset of Fig. 3). The parameter ΔS_{21} directly provides the intensity of the SAW signal at given frequencies, whilst the center frequency is given by the frequency at which ΔS_{21} reaches its maximum. The SAW
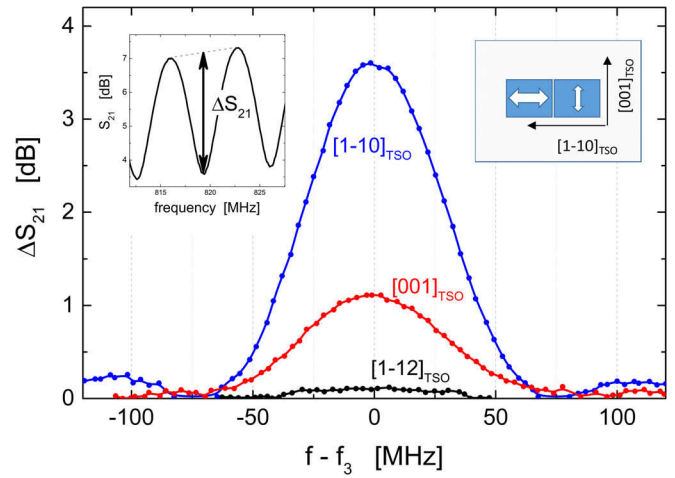

FIG. 3. Amplitude of the SAW signal ($\lambda = 12\,\mu$m and $L = 500\,\mu$m) at the 3rd harmonic at frequency f_3 for the different directions—$[1\bar{1}0]_{TSO}$, $[001]_{TSO}$, and $[1\bar{1}2]_{TSO}$—of the SAW propagation for a 27 nm-thick $(K_{0.7}Na_{0.3})NbO_3$ film on (110) $TbScO_3$ measured at room temperature. The insets sketch the definition of the amplitude ΔS_{21} (left) and the possible explanation of the anisotropy of the SAW signal (right) due to two types of domains with different polarizations in $[1\bar{1}0]_{TSO}$ and $[001]_{TSO}$ directions, respectively.[20]

bandwidth B is generally expected to be inversely proportional to the number of IDT cells[36] according to $B = 2f_o/N$, where f_o and N represent the fundamental frequency and the number of finger pairs, respectively. In our case, the expected bandwidth is (139 ± 3) MHz, which corresponds quite well with the experimental value $B \approx 138$ MHz observed for all directions.

However, the signal height is very different for the various directions. For example, ΔS_{21} is the largest for the SAW orientation along $[1\bar{1}0]_{TSO}$ ($\Delta S_{21}(f_3) = 3.6$ dB), whilst the maximum is significantly smaller ($\Delta S_{21}(f_3) = 1.1$ dB) along the direction $[001]_{TSO}$. For the intermediate direction $[1\bar{1}2]_{TSO}$, it is hardly measurable ($\Delta S_{21}(f_3) \approx 0.1$ dB). This means that SAWs propagate along the major crystallographic directions at different intensities but hardly do so in the intermediate direction. This anisotropic behavior could be explained by the polarization and structural anisotropy of the sample. In Ref. 20, it was shown that $K_{0.7}Na_{0.3}NbO_3$ films on (110) $TbScO_3$ develop a regular domain structure consisting of four variants of "superdomains" with domain wall alignment under $\pm45°$ with respect to $[001]_{TSO}$. Nevertheless, due to charge neutrality reasons, there are only two possible in-plane directions of the electrical polarization vector: P $\parallel [001]_{TSO}$ and P $\parallel [1\bar{1}0]_{TSO}$ (see sketch in Fig. 3). As a result, we only expect measurable SAW signals in these two directions. Furthermore, the polarizability and the development of SAWs are slightly different in the major directions $[001]_{TSO}$ and $[1\bar{1}0]_{TSO}$ due to the slight structural anisotropy of ~0.025% provided by the difference of the in-plane lattice parameter of the substrate. This difference is also visible in the measurements of permittivity and the resulting ferroelectric transition temperature, which are discussed within the context of Fig. 4.

Finally, Fig. 4 reveals the temperature dependence of the SAW signal at the 3rd harmonic and the corresponding permittivity for the different electric field and SAW propagation directions.
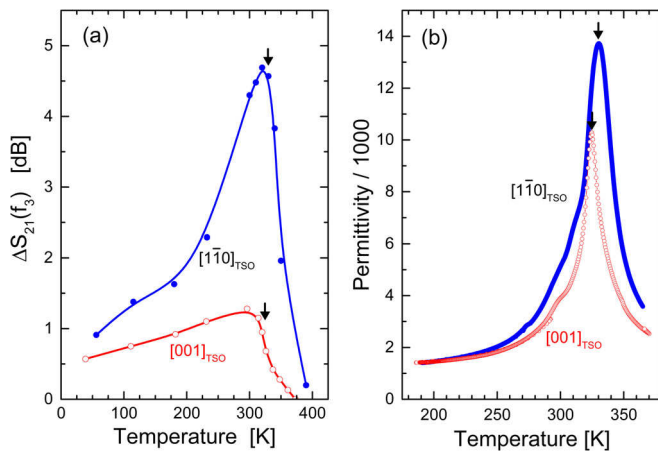
FIG. 4. Temperature dependence of the SAW signal ($\lambda = 12\,\mu m$ and $L = 500\,\mu m$) at the 3rd harmonic (a) and dielectric permittivity (b) for the different directions of the electric field and SAW propagation for a 27 nm-thick $(K_{0.7}Na_{0.3})NbO_3$ film on (110) TbScO$_3$. The arrows denote the temperature of the ferroelectric phase transition.

The permittivity measurements demonstrate the large polarizability of the $K_{0.7}Na_{0.3}NbO_3$ film. The temperature dependence resembles the typical behavior of a ferro-to-paraelectric transition with a peak in the permittivity ε at the transition temperature T_o. Due to the compressive stain, T_o is reduced from approximately 700 K for unstrained bulk $K_{0.7}Na_{0.3}NbO_3$[10,16,17] to 324 K and 330 K for the directions $[1\bar{1}0]_{TSO}$ and $[001]_{TSO}$, respectively. The reduction of T_o agrees with similar experiments on strained NaNbO$_3$[18,19] and the small difference in T_o obtained for both directions results from the small difference in the strain. As a result of the shift of T_o, the peak in the permittivity also shifts towards room temperature. For instance, a permittivity of $\varepsilon_{[001]} = 3970$ and $\varepsilon_{[1\bar{1}0]} = 5160$ is measured at room temperature, which rises up to $\varepsilon_{[001]} = 10270$ and $\varepsilon_{[1\bar{1}0]} = 13695$ at the respective T_o.

A similar behavior is visible in the SAW experiments [Fig. 4(a)]. The anisotropy is even more pronounced for the SAW signal compared to the permittivity measurement. For both major directions, the SAW signal $\Delta S_{21}(f_3)$ exhibits a maximum slightly below the ferroelectric phase transition T_o, reaching maximum values of 1.3 dB and 4.7 dB for the different directions. Since the transition temperature is adjusted via strain to a temperature slightly above room temperature, the room temperature values for $\Delta S_{21}(f_3)$ were found to be close to the maximum values. Above T_o, the SAW signal declines rapidly and finally vanishes slightly below 400 K.

In conclusion, thin epitaxial $K_{0.7}Na_{0.3}NbO_3$ films were grown on (110)TbScO$_3$ substrates exhibiting encouraging dielectric and piezoelectric properties. Permittivities of up to 13 700 and SAW signals of up to 4.7 dB were observed at the temperature around the ferroelectric phase transition. First, the SAW response of our only ~30 nm-thick films is very strong compared to that of other piezoelectric film systems,[6,34,37,38] which are typically several μm thick. Second, the phase transition temperature is shifted towards room temperature due to the compressive strain imposed on the film by the lattice mismatch between the film and the substrate, thus making these optimized ferroelectric properties accessible for room temperature applications. Finally, the ferroelectric properties were found to be strongly anisotropic. For instance, SAWs propagate along the major crystallographic directions—but not in the intermediate direction. Therefore, the strain-engineered thin epitaxial $K_{0.7}Na_{0.3}NbO_3$ films might be a promising way to adjust and optimize ferroelectric and piezoelectric properties for various room-temperature applications of ferroelectric films especially for highly sensitive sensors,[39,40] integrated microelectronics,[41] or hybrid systems.[42–46]

See supplementary material for the harmonic order dependence of the surface acoustic wave velocities.

[1]Y. Tang, D. Ao, W. Li, X. Zu, S. Li, and Y. Q. Fu, Sens. Actuators B: Chem. **254**, 1165 (2018).
[2]S. T. Ten, U. Hashim, S. C. B. Gopinath, W. W. Liu, K. L. Foo, S. T. Sam, S. F. A. Rahman, C. H. Voon, and A. N. Nordin, Biosens. Bioelectron. **93**, 146 (2017).
[3]M. Gillinger, K. Shaposhnikov, T. Knobloch, M. Schneider, M. Kaltenbacher, and U. Schmid, Appl. Phys. Lett. **108**, 231601 (2016).
[4]M. I. Gaso Rocha, Y. Jiмен́z, F. A. Laurent, and A. Arnau, in *Love Wave Biosensors: A Review, State of the Art in Biosensors-General Aspects*, edited by T. Rinken (InTech, 2013).
[5]X. Ding, S. C. S. Lin, B. Kiraly, H. Yue, S. Li, I. K. Chiang, J. Shi, S. J. Benkovic, and T. J. Huang, PNAS **109**, 11105 (2012).
[6]X. Y. Du, Y. Q. Fu, S. C. Tan, J. K. Luo, A. J. Flewitt, W. I. Milne, D. S. Lee, N. M. Park, J. Park, Y. J. Choi, S. H. Kim, and S. Maeng, Appl. Phys. Lett. **93**, 094105 (2008).
[7]B. Jaffe, R. S. Roth, and S. Marzullo, J. Appl. Phys. **25**, 809 (1954).
[8]European Union, "Directive 2002/95/EC of the European Parliament and of the Council of 27 January 2003 on the restriction of the use of certain hazardous substance in electrical and electronic equipment," Off. J. Eur. Union **L37**, 19 (2003).
[9]Y. Guo, K. Kakimito, and H. Ohsato, Appl. Phys. Lett. **85**, 4121 (2004).
[10]E. Hollenstein, M. Davis, D. Damjanovic, and N. Setter, Appl. Phys. Lett. **87**, 182905 (2005).
[11]N. Klein, E. Hollenstein, D. Damjanovic, H. J. Trodahl, N. Setter, and M. Kuball, J. Appl. Phys. **102**, 014112 (2007).
[12]D. Lin, K. W. Kwok, and H. L. W. Chan, J. Appl. Phys. **102**, 034102 (2007).
[13]K. Wang, J. F. Li, and N. Liu, Appl. Phys. Lett. **93**, 092904 (2008).
[14]Y. Saito, H. Takao, T. Tani, T. Nonoyama, T. Takatori, T. Homma, T. Nagaya, and M. Nakamura, Nature **432**, 84 (2004).
[15]J. Schwarzkopf, D. Braun, M. Hanke, R. Uecker, and M. Schmidbauer, Front. Mater. **4**, 26 (2017).
[16]M. Matsubara, T. Yamaguchi, K. Kikuta, and S. Hirano, Jpn. J. Appl. Phys. **43**, 7159 (2004).
[17]G. Z. Zang, J. F. Wang, H. C. Chen, W. B. Su, C. M. Wang, P. Qi, B. Q. Ming, J. Du, and L. M. Zheng, Appl. Phys. Lett. **88**, 212908 (2006).
[18]R. Wördenweber, J. Schwarzkopf, E. Hollmann, A. Duk, B. Cai, and M. Schmidbauer, Appl. Phys. Lett. **103**, 132908 (2013).
[19]B. Cai, J. Schwarzkopf, E. Hollmann, M. Schmidbauer, M. O. Abdel-Hamed, and R. Wördenweber, J. Appl. Phys. **115**, 224103 (2014).
[20]L. von Helden, M. Schmidbauer, S. Liang, C. Feldt, M. Hanke, R. Wördenweber, and J. Schwarzkopf, "Ferroelectric Monoclinic Phases in Strained $K_{0.70}Na_{0.30}NbO_3$ Thin Films Promoting Selective Surface Acoustic Wave Propagation," Nanotechnology (published online).
[21]R. Uecker, B. Velickov, D. Klimm, R. Bertram, M. Bernhagen, M. Rabe, M. Albrecht, R. Fornari, and D. G. Schlom, J. Cryst. Growth **310**, 2649 (2008).
[22]A. R. Denton and N. W. Ashcroft, Phys. Rev. A **43**, 3161 (1991).

[23]A. G. Kalinichev, J. D. Bass, C. S. Zha, P. D. Han, and D. A. Payne, J. Appl. Phys. **74**, 6603 (1993).

[24]L. Wu, J. L. Zhang, C. L. Wang, and J. C. Li, J. Appl. Phys. **103**, 084116 (2008).

[25]R. Wördenweber, J. Schubert, T. Ehlig, and E. Hollmann, J. Appl. Phys. **113**, 164103 (2013).

[26]O. G. Vendik, S. P. Zubko, and M. A. Nikol'ski, Tech. Phys. **44**, 349 (1999).

[27]C. C. Tseng, IEEE Trans. Electron Devices **ED-15**, 586 (1968).

[28]R. M. White, Proc. IEEE **58**, 1238 (1970).

[29]W. R. Smith, H. M. Gerard, J. H. Collins, T. M. Reeder, and H. J. Shaw, IEEE Trans. Microwave Theory Tech. **17**, 856 (1969).

[30]Y. Sakshita and H. Segawa, J. Appl. Phys. **77**, 5995 (1995).

[31]C. R. Gorla, N. W. Emanetoglu, S. Liang, W. E. Mayo, Y. Lu, M. Wraback, and H. Shen, J. Appl. Phys. **85**, 2595 (1999).

[32]W. L. Dang, Y. Q. Fu, J. K. Luo, A. J. Flewitt, and W. I. Milne, Superlattices Microstruct. **42**, 89 (2007).

[33]T. T. Wu and W. S. Wang, J. Appl. Phys. **96**, 5249 (2004).

[34]X. Y. Du, Y. Q. Fu, S. C. Tan, J. K. Luo, A. J. S. Maeng, S. H. Kim, Y. J. Choi, D. S. Lee, and N. M. Park, J. Phys.: Conf. Ser. **76**, 012035 (2007).

[35]Y. Takagaki, P. V. Santos, E. Wiebicke, O. Brandt, H.-P. Schönherr, and K. H. Ploog, Appl. Phys. Lett. **81**, 2538 (2002).

[36]D. S. Ballantine, R. M. White, S. J. Martin, A. J. Ricco, E. T. Zellers, G. C. Frye, and H. Wohltjen, *Acoustic Wave Sensors, Theory, Design and Physico-Chemical Applications* (Academic Press, 1997).

[37]T. Mino, S. Kuwajima, T. Suzuki, I. Kanno, H. Kotera, and K. Wasa, Jpn. J. Appl. Phys., Part 1 **46**, 6960 (2007).

[38]D. Damjanovic, Rep. Prog. Phys. **61**, 1267 (1998).

[39]K. länge, B. E. Rapp, and M. Rapp, Anal. Bioanal. Chem. **391**, 1509 (2008).

[40]A. Mujahid and F. L. Dickert, Sensors **17**, 2716 (2017).

[41]Y. Q. Fu, J. K. Luo, N. T. Nguyen, A. J. Walton, A. J. Flewitt, X. T. Zu, Y. Li, G. McHale, A. Matthews, E. lborra, H. Du, and W. I. Milne, Prog. Mater. Sci. **89**, 31 (2017).

[42]V. Sampath, N. D'Souza, D. Bhattacharya, G. M. Atkinson, S. Bandyopadhyay, and J. Atulasimha, Nano Lett. **16**, 5681 (2016).

[43]E. D. S. Nysten, Y. H. Huo, H. Yu, G. F. Song, A. Rastelli, and H. J. Krenner, J. Phys. D: Appl. Phys. **50**, 43LT01 (2017).

[44]Y. Chen, X. Ding, S. S. Lin, S. Yang, P. Huang, N. Nama, Y. Zhao, A. A. Nawaz, F. Guo, W. Wang, Y. Gu, T. E. Mallouk, and T. J. Huang, ACS Nano **7**, 3306 (2013).

[45]T. Lin, C. Lin, and J. Hsu, Sci. Rep. **5**, 13782 (2015).

[46]M. V. Gustafsson, T. Aref, A. F. Kockum, M. K. Ekström, G. Johansson, and P. Delsing, Science **346**, 207 (2014).